Original article

Experimental study on production characteristics and enhanced oil recovery during imbibition and huff-n-puff injection in shale reservoir

Jianguang Wei[1,2], Demiao Shang[2], Xiaoqing Zhao[1,2], Xiaofeng Zhou[1,2], Ying Yang[1,2]⊙*, Meng Du[3]

[1]*State Key Laboratory of Continental Shale Oil, Northeast Petroleum University, Daqing 163318, P. R. China*
[2]*Institute of Unconventional Oil & Gas, Northeast Petroleum University, Daqing 163318, P. R. China*
[3]*School of Engineering Science, University of Chinese Academy of Sciences, Beijing 100049, P. R. China*

Abstract:
Imbibition and huff-n-puff injection in shale reservoirs can significantly enhance oil recovery after depletion. To clarify the microscopic production characteristics and enhance the oil recovery mechanisms across different pore scales during imbibition and huff-n-puff injection, this study establishes an online physical simulation method that integrates imbibition and huff-n-puff using nuclear magnetic resonance and conducts a series of online nuclear magnetic resonance analyses under different imbibition systems. The microscopic production characteristics and dynamic development characteristics are quantitatively studied from the aspects of pore recovery and residual oil distribution. The results show that the occurrence states of pores of shale oil can be categorized into three types, including adsorption pore as the predominant type, followed by percolation pore and migration pore. When viewing the entire imbibition process comprehensively, it becomes imperative to maximize the recovery of migration pores while ensuring the recovery degree of adsorption pores. The recovery of free oil increases with the imbibition amount and the residual oil gradually shifts to adsorbed and organic matter-dominated forms, resulting in gradually decreasing recoverability. Using water-based imbibition media achieves a superior production effect for adsorbed oil in interlayered clay, whereas CO_2 imbibition media can effectively improve the recovery of organic matter through mass transfer, leading to 11.01%-23.54% enhancement in oil recovery. Leveraging the bridge flow conductivity of fractures, fluid imbibition displacement and CO_2 carrying effect emerges as a pivotal strategy for achieving optimal enhanced oil recovery.

1. Introduction

As a pivotal alternative energy resource for augmenting crude oil reserves and production, shale oil primarily refers to the oil occurring within micro-nanoscale organic-rich shale formations (Afagwu et al., 2022; Wang et al., 2023; Zhou et al., 2024). Shale oil has emerged as a strategic reserve within China's oil fields, positioned to augment production (Lv et al., 2019; Du et al., 2022; Andersen, 2023). Nevertheless, the pore throat structure of shale reservoirs in China are of the continental sedimentary type, whose complexity results in generally low initial recovery (Jin et al., 2017, 2021). The recent adoption of horizontal well scale fracturing technology has effectively induced numerous artificial fractures, enhancing the near-well seepage capacity and bolstering single-well production (Qin et al., 2023; Wei et al., 2023a; Zhou et al., 2023; Jin et al., 2024). Despite these advancements, the large difference in the seepage capacity of matrix fractures continues to complicate conventional gas or water flooding, as fluid tends to preferentially follow the fracture path. Con-

sequently, there is an urgent need to explore more advanced and efficient development methodologies.

Many studies have shown that imbibition is an essential principle of enhanced oil recovery (EOR) in shale reservoirs (Bocangel et al., 2013; Ghandi et al., 2019; Fakher and Imqam, 2020; Cai et al., 2021a). The fluid can be expelled by capillary force, thereby achieving EOR (Yang et al., 2019; Guo et al., 2021; Gao et al., 2023; Li et al., 2024). Extensive evidence also suggests that CO_2 huff-n-puff (HNP) injection is very important for improving oil recovery after depletion, since gas channeling can be effectively avoided and pressure can be recovered periodically, offering favorable economic benefits and high recovery rates (Wang et al., 2022; Huang et al., 2023). Consequently, it is imperative to explore the intricate mechanism of oil-water-gas multiphase flow in the matrix-fracture interface and assess the imbibition-displacement and CO_2 dissolution extraction effect during the imbibition and HNP process. Many efforts have been made to research imbibition and HNP, mainly focusing on the imbibition production characteristics, the law of CO_2 HNP increasing production and the influencing factors by the physical simulation method (Liu et al., 2021, 2024; Huang et al., 2023; Hosseini et al., 2024). Hu et al. (2020) systematically summarized the development mechanism of imbibition and analyzed the water-rock interaction through laboratory experiments. Guo et al. (2021) investigated the impact of thermodynamic variables on dynamic imbibition and scrutinized the migration behavior of crude oil in various shale cores during this process. Zhang et al. (2022) confirmed the contribution of three pore types to recovery during imbibition under different in-situ stress conditions and highlighted the predominant role of seepage pores and migration pores in oil recovery. Lai et al. (2019) examined the microscopic production characteristics and investigated the fluid distribution in porous media during imbibition. Xiong et al. (2022) analyzed the impact of reservoir physical properties on imbibition and CO_2 HNP. They concluded that superior reservoir quality leads to better pore throat connectivity and displacement effects. The above studies mostly employed traditional experimental equipment, hence accurately measuring the volume of oil adsorbed on the sample particle surfaces during imbibition remains challenging. To this end, some scholars applied imbibition microfluidics and numerical simulation to explore the production characteristics of shale oil dynamic imbibition. Wang et al. (2017) established a mathematical model of imbibition based on imbibition theory and studied the effects of matrix permeability, interfacial tension and rock size on dynamic imbibition recovery through laboratory experiments. Nguyen et al. (2018) conducted microfluidic experiments to quantitatively analyze the effect of fractures on recovery. However, these studies often rely on ideal models, which may differ significantly from the real porous media of shale cores and the conclusions are not always robust (Zhao et al., 2018; Wei et al., 2023b). In contrast, Sharma et al. (2012) deduced an imbibition scale model, then quantitatively described the complex exchange dynamics in the imbibition process. Nevertheless, the microscopic oil migration and production characteristics of imbibition and CO_2 HNP have not been fully elucidated, warranting further

research.

In recent years, some studies have made advancements in the visualization and quantitative assessment of oil saturation distribution within matrix pores and fractures during imbibition or HNP (Singh and Cai, 2018; Fang et al., 2023; Li et al., 2023). Nuclear magnetic resonance (NMR) is recognized as a crucial method for the accurate and quantitative evaluation of microscopic production characteristics and multiphase flow within various cores. Dai et al. (2019) discussed the production characteristics of crude oil from nanopores to micron-scale pores during imbibition. Gu et al. (2017) conducted physical simulation experiments on dynamic imbibition, employing CT scanning and NMR to explore the microscopic seepage and the influence of tight core permeability on imbibition-assisted oil recovery. Wang et al. (2020) conducted an experiment of dynamic imbibition under high pressure and revealed its influence on tight oil exploitation from the pore-scale perspective. Guo et al. (2016) studied the key factors of spontaneous imbibition of fracturing fluid and its oil/water displacement and determined the optimal imbibition recovery and maximum imbibition efficiency. Li et al. (2019) developed an imbibition kinetic model for pores of different scales via NMR, introducing the water absorption constant to characterize the dynamic imbibition effects. The current research methods for the analysis of shale oil occurrence mainly include conventional pyrolysis, laser confocal microscopy and molecular dynamics simulation (Bocangel et al., 2013). However, these methods are limited to analysis from the perspective of EOR development. Minh et al. (2012) used 2-dimensional (2D) NMR to categorize the occurrence state of shale oil into kerogen, free state and partially swollen state, with the free state primarily occurring in macropores and microfractures of the core and the adsorbed state mainly present in clay interlayer minerals and kerogen organic matter surfaces. Xu et al. (2023) analyzed fluid occurrence and its contribution to recovery under different stages of CO_2 HNP in tight reservoirs. In summary, the current research predominantly focuses on the kinetic characteristics of imbibition and HNP recovery, while few scholars have delved into the microscopic production characteristics and EOR mechanisms of shale reservoir imbibition and HNP concerning microscopic pore-scale recovery and residual oil distribution. In particular, the quantitative characterization of dynamic development characteristics should be performed at different stages and the contribution mechanism of oil occurrence state to EOR based on 2D NMR needs to be further analyzed.

To address the above issues, we carried out online NMR experiments of imbibition and HNP under different systems. By monitoring the production process of crude oil in real time, we quantified the microscopic production characteristics of different levels of pore oil. In addition, we constructed a novel 2D NMR interpretation model to study the contribution of different oil occurrence pores to EOR. Subsequently, we elucidated the dynamic development characteristics of shale oil integrated injection-imbibition-soaking-production and explored multiscale oil migration seepage mechanism models. The distinctiveness of our study lies in its consideration of the microscopic production characteristics of imbibition and CO_2
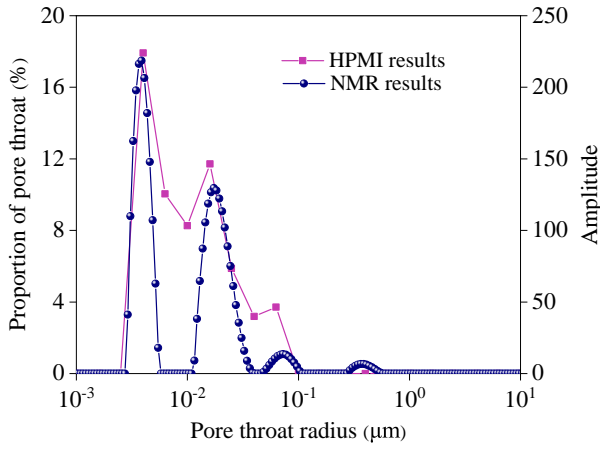
Fig. 1. Pore throat scale distribution and the time-space conversion coefficient calibration process.

HNP from a pore-scale quantification perspective, which can provide an engineering theoretical basis for the development of shale oil.

2. Experimental settings

2.1 Online NMR imbibition-HNP experimental method

Nuclear magnetic resonance testing is carried out mainly by analyzing the interaction between the nucleus in the fluid and the applied magnetic field (Zhang et al., 2022). Under the action of magnetic field force, the fluid hydrogen proton is proportional to the signal quantity. Numerous studies have indicated that the characteristic parameters of fluid can be presented by the time constant T_2 (Gu et al., 2017). The T_2 and pore throat radius can be accurately calibrated through high-pressure mercury injection experiments. Fig. 1 displays the pore throat distribution and the time-space conversion coefficient calibration process obtained from parallel shale samples, which reveals a primarily bimodal distribution that is concentrated in the 0.005-1.000 μm range. Moreover, the T_2 spectrum of core oil saturation can be derived through NMR testing. The expression of T_2 relaxation time is as follows:

$$M(t) = \sum_i A_i \exp\left(-\frac{t}{T_{2i}}\right) \tag{1}$$

where $M(t)$ denotes the inversion of total semaphore, dimensionless, $A(i)$ denotes the cumulative total signal amplitude, dimensionless, T_{2i} denotes the ith relaxation time, ms:

$$\frac{1}{T_2} = \frac{1}{T_{2B}} + \frac{1}{T_{2S}} + \frac{1}{T_{2D}} \tag{2}$$

In Eq. (2):

$$\frac{1}{T_{2S}} = \rho_2 \left(\frac{S}{V}\right)_{\text{pore}} \tag{3}$$

where T_2 denotes the relaxation time, ms; T_{2B} and T_{2S} denote the transverse relaxation times of the filling fluid and rock particle surface, ms, respectively; T_{2D} denotes the transverse relaxation time caused by fluid diffusion in magnetic field gradients, ms.

T_{2B} and T_{2D} can often be ignored in the actual test, hence the T_2 relaxation time can also be expressed as:

$$\frac{1}{T_2} = \rho_2 \left(\frac{S}{V}\right)_{\text{pore}} = F_s \left(\frac{\rho_2}{r_c}\right) \tag{4}$$

Therefore, the relationship between pore radius and T_2 can be expressed as:

$$r_c = \rho_2 F_s T_2 \tag{5}$$

$$r_c = C T_2 \tag{6}$$

where ρ_2 denotes the surface relaxation strength, μm/ms, S denotes the pore surface area, cm^2, V denotes the pore volume, cm^3, F_s is the pore geometry factor (spherical pore, $F_s = 3$; columnar pore, $F_s = 2$;), r_c denotes the pore size, cm, and C is the NMR time-space conversion coefficient.

Finally, the time-space coefficient of conversion from T_2 to pore throat radius is computed by integrating the experimental results of high-pressure mercury intrusion. From the data, it is evident that the pore throat radius conversion results have high correlation.

2.2 Experimental apparatus and materials

2.2.1 Apparatus

In order to facilitate studies on imbibition in shale reservoirs, we developed an online NMR experimental apparatus (Fig. 2). It is mainly composed of an NMR unique core holder, back pressure pump, confining pressure pump and an ISCO constant-speed constant-pressure displacement pump. The instrument model is MacroMR12 (NiuMai, Co., China), with a frequency of 12.798 MHz. 2D NMR scanning tests can be realized based on 1-dimensional (1D) NMR and the minimum echo time can effectively detect the nanometer signal.

2.2.2 Materials

The experimental shale samples were sourced from the Liaohe Oilfield. The porosity and permeability of the six shale core samples subjected to experimentation ranged from 8.1% to 9.3% (average 8.4%) and 0.021 to 0.032 mD (average 0.025 mD), respectively. The physical parameters of these cores are shown in Table 1. To present the effect of fractures on imbibition, the Y5 matrix core was used as a comparison and the Y6 cores were artificially fractured according to 2/3 the length of the sample. The imbibition liquid medium employed in the experiment was an acidic low-viscosity slick water (ASW) system (0.2% thickener + 0.25% cleanup additive + 0.5% anti-swelling agent + 0.05% breaker, pH = 1.5). The anti-swelling agent was used to prevent shale from swelling by water absorption. The guar gum gel breaking solution (GBS) system contained base solution (0.35% guar gum + 0.25% cleanup agent+0.5% anti-swelling agent) + tablet alkali + 0.25% crosslinking agent + 0.05% gel breaking agent. The CO_2 imbibition solution system contained 99.999% CO_2 purity + simulated formation water with a salinity of 9,758 mg/L. The surfactant type acidic low-viscosity slick water (S+ASW) system had a slippery water formula of 0.2% thickener+0.25%
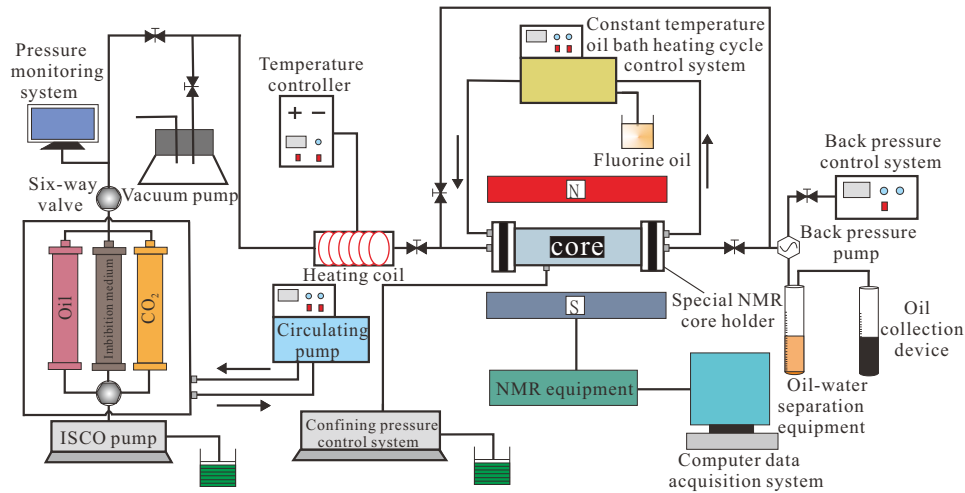
Fig. 2. Schematic diagram of the proposed online NMR imbibition-HNP dynamic physical experimental apparatus.

Table 1. Core sample information of online NMR experiments.

Sample	Diameter (cm)	Length (cm)	Porosity (%)	Permeability (mD)	Imbibition system	Depth (m)
Y1	2.495	8.935	8.3	0.023	Acidic low-viscosity slick water	1,980.5-1,990.6
Y2	2.501	8.917	7.9	0.021	Guar gum gel breaking solution	1,985.5-1,990.7
Y3	2.498	8.945	8.5	0.028	CO_2 imbibition solution	1,987.5-1,995.3
Y4	2.497	8.937	8.1	0.024	Surfactant type acidic low-viscosity slick water	1,988.5-1,995.5
Y5	2.492	8.942	8.4	0.021	Acidic low-viscosity slick water+CO_2	1,985.5-1,991.3
Y6 (Fractured)	2.502	8.968	9.3	0.032	Acidic low-viscosity slick water+CO_2	1,988.5-1,993.5

cleanup additive + 0.5% anti-swelling agent + 0.05% breaker and the surfactant was nano-emulsion surfactant. To facilitate the analysis and description of the imbibition effect and the oil displacement characteristics of different systems, the above four systems are referred to as ASW system, GBS system, CO_2 system and S+ASW system in this paper. In addition, to simulate the development of shale oil under actual formation conditions, the experimental oil was taken from the Liaohe shale reservoir and the viscosity and density of the oil under formation conditions were 8.671 mPa·s and 0.885 g/cm³, respectively.

2.3 Experimental procedure

The real-time 1D NMR T_2 spectra and T_1-T_2 2D NMR spectra of shale imbibition were monitored and obtained through the online NMR system. The online NMR imbibition experimental procedures were as follows:

1) Core pretreatment: The core was dried for 24 h after being washed with oil and salt. It was then placed in a unique holder and the 1D and 2D NMR spectra of the dry core were tested by scanning the dry sample.
2) Oil saturation treatment: First, the experimental core was evacuated; then, the experimental temperature was set to 95 °C and the crude oil was saturated by high pressure; finally, the aging process was carried out. The 1D and 2D NMR spectra of the saturated oil core were determined by NMR equipment. The core oil saturation was calculated by the weighing method and spectral line change.

3) Imbibition development: The system pressure was set to the reservoir pressure and the confining pressure was set to a tracking mode of 3 MPa higher than the injection end. The imbibition liquid (ASW system) was injected into the core, the NMR scanning was performed at different imbibition times (48, 96, 144, 192 h) and the residual oil distribution was observed. The experiment was completed when the spectral line stabilized and the different pore recovery and total recovery were calculated by statistically analyzing the amplitude changes of the 1D and 2D NMR spectra.

4) The experimental steps 1)-3) were repeated under different imbibition liquid media (GBS system, CO_2 system and S+ASW system). To ensure the reliability and accuracy of the experimental data, the nuclear magnetic equipment was calibrated with standard cores.
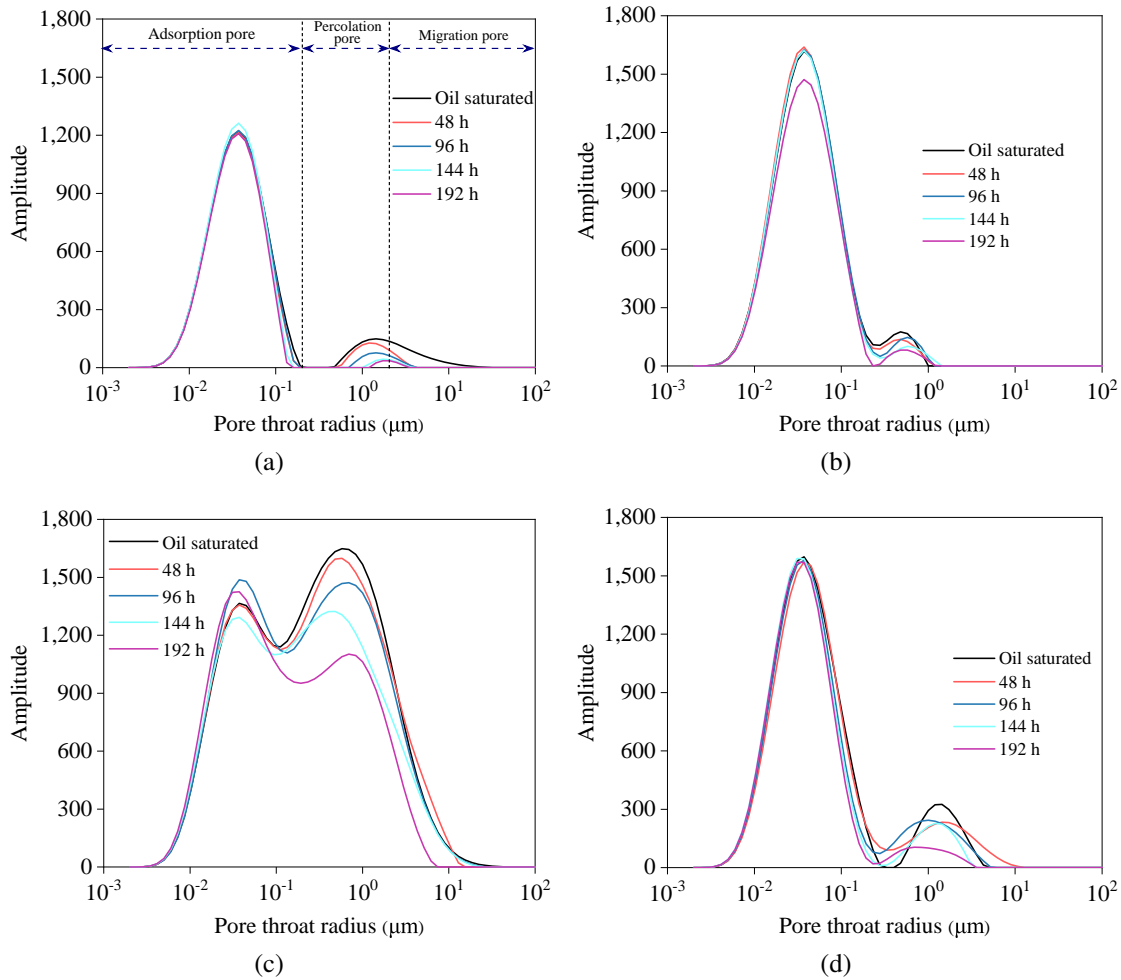
Fig. 3. Evolution of NMR T_2 spectra during imbibition under different imbibition systems. (a) ASW system, (b) GBS system, (c) CO_2 system and (d) S+ASW system.

To further study the full-cycle dynamic development characteristics and EOR mechanism of integrated injection-imbibition-soaking-production, based on the above online NMR experimental system, samples Y5 and Y6 were taken to conduct the integrated dynamic seepage experiment of imbibition coupling HNP development. The underground seepage of shale reservoir fluid was reproduced and the following experimental procedures were performed:

1) According to the above experimental steps 1)-2), the core was dried for 24 h after being washed with oil and salt and the 1D and 2D NMR spectra of the corresponding states were obtained. The confining pressure was set to a tracking mode of 3 MPa higher than the injection end. The imbibition liquid (ASW system) was injected into the core and the contact between the core and the imbibition medium was realized. The NMR scanning was performed at different imbibition times (48, 96, 144, 192 h) and the residual oil distribution was observed.

2) The 1D and 2D NMR spectra at the end of imbibition development were obtained after the imbibition was no longer producing oil. The valve at the outlet end of the

holder was closed and CO_2 was injected into the holder at a preset pressure. When the system pressure was stable at 28 MPa, the valve at the inlet end was closed. In the soaking stage, CO_2 is in full contact with the crude oil in the core and reacts with it. The NMR test was carried out when the soaking time was 15 and 25 h and the distribution of crude oil in the soaking process was analyzed.

3) When the soaking stage was over, the inlet valve was opened and the injection pressure was gradually decreased to 20, 15, 8 and 0 MPa. The, the controlled-pressure HNP development was carried out. When the pressure in the system gradually decreased to atmospheric pressure and oil was no longer produced, the HNP experiment was completed. The 1D and 2D spectra were obtained and the dynamic production characteristics of crude oil in the process of HNP development were analyzed.

4) The experimental steps 1)-3) were repeated under different types of cores and the dynamic development characteristics of different types of cores were investigated.

3. Results and analysis

3.1 Pore oil production and effects of imbibition based on 1D NMR

Fig. 3 displays the NMR T_2 spectra of four shale cores under various imbibition systems. The analysis of the T_2 spectrum distribution of shale saturated oil (illustrated by the black line in Fig. 3) reveals that pore scales were primarily distributed in the range of 0.01-10.00 μm, with the NMR T_2 spectrum mainly manifesting in the form of double peaks. Based on the occurrence space of crude oil, the T_2 spectrum trough of shale samples was observed near $T_2 = 10$ ms (200 nm) and $T_2 = 100$ ms (2,000 nm). Consequently, the occurrence pores of crude oil could be categorized into three groups: Those with T_2 values of < 10 ms, 10-100 ms and >100 ms, representing adsorption pores (< 0.2 μm) (AP), percolation pores (0.2-2.0 μm) (PP) and migration pores (> 2.0 μm) (MP), respectively.

According to the NMR T_2 spectra, the recovery of different levels of pore oil could be quantified (Table 2). As imbibition time progresses, the nuclear magnetic signals of pores in the T_2 spectrum undergo significant changes, with both the peak value and the peak area of the spectrum decreasing, indicating a reduction in oil content within the core. At 48 h of imbibition time, the envelopes corresponding to the MP of the four cores indicate a significant reduction, suggesting that MP significantly contributes to oil recovery under capillary force. Upon reaching 96 h of imbibition, the amplitude associated with MP continues to decline, while the signal of PP decreases to a certain extent, with no noticeable change in the left peak. This means that the imbibition fluid initially triggers oil production in PP and MP. The pore throat structure gradually transforms into heterogeneous seepage and diffusion channels, with PP and MP becoming the primary contributors to oil production. Subsequently, as the imbibition time reaches 144 h, the T_2 spectrum peak gradually shifts leftward, the envelope line narrows and decreases significantly and the AP spectrum gradually decreases. This indicates an increase in the lower limit of pore throat production, with crude oil evolving into a scattered discontinuous phase and AP becoming the predominant production pores, increasing AP recovery. Upon further extending the imbibition time to 192 h, the change of the spectral line is very small, which indicates that the oil production is weak. It is noteworthy that under CO_2 system imbibition, the T_2 reduction amplitude is the largest for the same imbibition time and not only does MP exhibit higher imbibition recovery but also PP and AP achieve higher recovery.

Collectively, the findings suggest that the production rate during imbibition is more pronounced in the early stages, gradually tapering off in the later stages. The NMR T_2 spectra (0.02-10.00 μm), which represent the primary pore range yielding production during core imbibition, correspond to pores with durations of 1-500 ms, with AP and MP primarily governing residual oil. The related recovery of the ASW system, GBS system, CO_2 system and S+ASW system was measured as 16.13%, 11.80%, 21.00% and 14.68%, respect-

Table 2. Online NMR results of imbibition in shale samples.

Sample	Time (h)	Total recovery degree (%)	Proportion of recovery degree (%)		
			AP	PP	MP
Y1	48	7.13	1.89	1.95	3.28
	96	8.59	0.59	4.68	3.33
	144	10.99	1.09	6.44	3.46
	192	16.13	5.82	6.78	3.54
Y2	48	0.40	-0.44	0.85	0
	96	1.09	0.19	0.90	0
	144	3.26	1.41	1.85	0
	192	11.80	9.09	2.71	0
Y3	48	1.58	0.52	1.93	-0.88
	96	3.93	-0.91	4.42	0.42
	144	12.72	1.66	10.05	1.01
	192	21.00	1.30	15.20	4.49
Y4	48	0.83	2.51	0.21	-1.88
	96	4.39	5.16	-0.73	-0.03
	144	8.72	5.14	2.69	0.89
	192	14.68	7.76	6.00	0.92

ively. The imbibition recovery of the GBS system was the weakest and the imbibition effect of the ASW system demonstrated a declining trend with the addition of surfactant, while the CO_2 system exhibited the most favorable results. It is hypothesized that the high-pressure CO_2 solution can reduce interfacial tension, allowing the CO_2 imbibition liquid to penetrate different pore levels for oil production, thereby significantly enhancing the total recovery.

3.1.1 Pore oil production during imbibition in shale core

Taking samples Y1 and Y3 corresponding to the ASW system and CO_2 system as examples, Fig. 4(a) depicts the correlation between the pore oil recovery degree and imbibition time based on the NMR T_2 spectra, revealing distinct production characteristics among pores of varying scales. It can be observed that when the ASW or CO_2 imbibition liquid infiltrates the core, oil is initially produced in the percolation pores and migration pores. Consequently, the oil recovery degree of PP exhibits a slowly increasing trend, while that of MP shows an initial slow increase followed by rapid escalation, gradually enhancing the recovery degree. The fluctuating trend in the recovery degree of adsorption pores is particularly noteworthy; it is characterized by an initial decrease followed by an increase, which is due to two factors: (1) The migration of AP oil during the ASW system imbibition process results in oil redistribution and (2) the high-pressure leads to the significant volatility of CO_2. This enables CO_2 to transport matrix oil to nanoscale AP, causing the redistribution
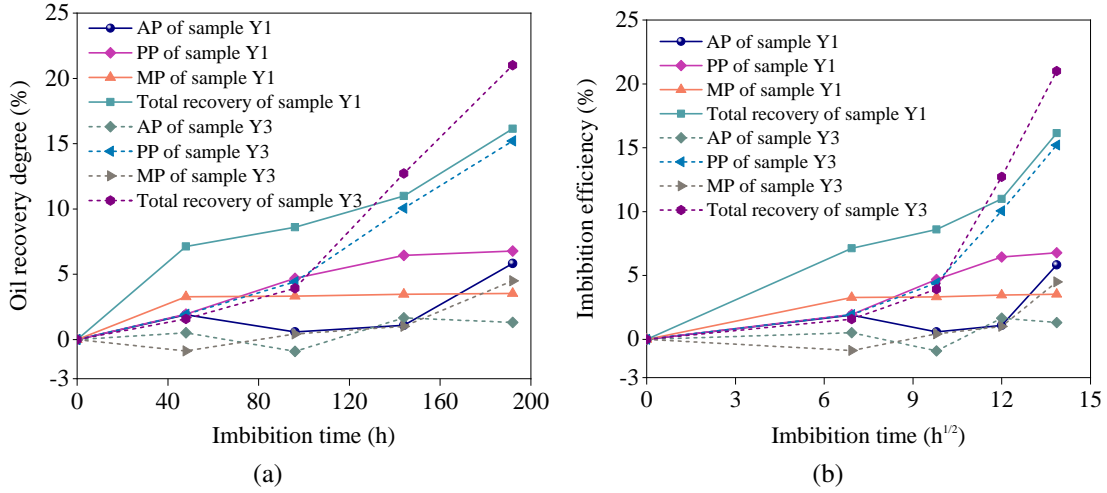
Fig. 4. Relationship between (a) pore oil recovery degree and (b) imbibition efficiency with time during imbibition.

of crude oil within AP.

Furthermore, the imbibition process can be effectively described and modeled using the L-W classical imbibition model (Washburn, 1921). This model assumes that the imbibition process of porous media is mainly dominated by uniform piston motion. The imbibition mass equation in porous media can be expressed as:

$$W_{L-W} = \rho A \phi \sqrt{\frac{\sigma r \cos\theta}{2\mu} t} \qquad (7)$$

The micro-nano pore throat structure of actual shale reservoirs is extremely complex, often characterized by poor uniformity in pore throat size. Obtaining an accurate average pore throat radius for the L-W imbibition model has proved challenging. Based on Darcy's formula and Poiseuille's law, Xu et al. (2023) performed a fitting process to the relationship between the average pore throat radius and reservoir permeability, thereby optimizing the L-W imbibition model. The optimized expression is presented as follows:

$$r = \tau \sqrt{\frac{8K_a}{\phi}} \qquad (8)$$

Therefore, the mass of imbibition recovery during imbibition can be expressed as:

$$W_{L-W} = \rho A \left(2K_a \phi^3\right)^{\frac{1}{4}} \sqrt{\frac{\tau \phi \cos\theta}{\mu} t} \qquad (9)$$

where W_{L-W} denotes the imbibition mass, g; ρ denotes the fluid density, kg/m³; A denotes the contact area between porous media and fluid, m²; ϕ denotes the porosity, %; σ denotes the interfacial tension, N/m; θ denotes the contact angle, °; μ denotes the viscosity of imbibition liquid, Pa·s; t denotes the imbibition time, h; K_a denotes the permeability, m²; r denotes the average pore throat radius, m; τ denotes the porous medium pore curvature, dimensionless.

According to Eq. (9), under the same conditions, reservoir imbibition recovery is positively correlated with porosity, permeability and contact angle. Furthermore, the amount of imbibition is proportional to the square root of time in the imbibition process. As depicted in Fig. 4(b), the slope of the curve indicates the imbibition rate, with the Y1 and Y3 samples demonstrating a positive correlation between imbibition efficiency and the square root of time. During the initial stage of imbibition (0-96 h), the slopes of the curves for the three types of pores and the total pore imbibition efficiency are relatively small, suggesting a slower imbibition rate. On the other hand, in the later stage of imbibition (96-192 h), the slopes of PP, MP and total pore curves are steeper, signifying a gradual enhancement in imbibition rate, consistent with the preceding analysis.

The above results suggest that when the imbibition liquid enters the core, it first enters PP and MP to produce oil because of its lower seepage resistance. Subsequently, a crossflow of oil and water transpires between matrix fractures due to the pressure differential. Owing to the combined effects of pressure difference and imbibition capillary force, imbibition liquid can enter the fracture to displace oil. As a result, the MP oil and some AP oil are effectively produced, promoting total recovery. When the pressure in the MP can overcome the seepage resistance in PP and AP, the imbibition liquid will enter the next level of pores to produce oil. Meanwhile, as the pressure drop gradually shifts to PP and AP, the oil difficult to be produced in PP and AP can flow to MP and migrate to the oil production end through MP, which makes MP act as the primary oil migration channel in the process of imbibition. Due to the continuous migration of MP oil, the amplitude of the internal hydrogen signal fluctuates, which explains why the recovery of MP is lower and shows a trend of floating up and down.

For the oil production of AP, the imbibition liquid first carries part of the oil into AP, resulting in its negative recovery. Subsequently, under the influence of wettability, retained fluid continuous migration in PP and MP spontaneously imbibe into AP along the particle surfaces, stripping the oil film from the pore walls. Moreover, the thickening of water film on the
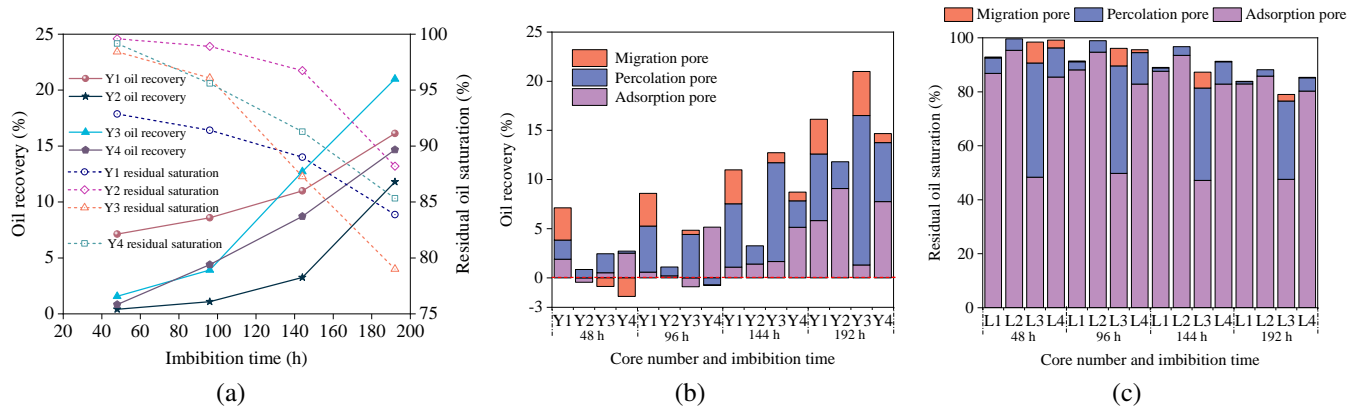
Fig. 5. Relationship between (a) oil recovery, (b) imbibition efficiency and (c) residual oil saturation with time under different imbibition systems.

pore wall also causes the oil phase in AP to be squeezed and produced (Du et al., 2022). This process is predominantly characterized by reverse imbibition in AP, with AP becoming the main contributor to total recovery. Compared with the ASW system, the CO_2 system exhibits a significantly larger diffusion capacity than the liquid phase, facilitating its entry into AP and PP through diffusion, thereby expanding the CO_2 sweep area and enhancing the imbibition efficiency.

Overall, it can be concluded that the capillary force between the oil and the water phase in PP and MP has a positive effect, providing AP with imbibition power and thus expanding the sweep efficiency. Essentially, the entire imbibition process resembles an organic system; that is, the AP oil produced by imbibition is discharged to the production end through large pores or fractures and the specific imbibition power is beneficial to MP recovery. However, insufficient imbibition power hinders the effective use of MP oil, disrupting the flow of AP oil to MP and reducing the recovery of both pore types as well as the overall recovery. Hence, to maximize EOR, improving the effect of MP while ensuring the recovery degree of AP is crucial.

3.1.2 Pore oil production effect of imbibition in different systems

The relationship between oil recovery and residual oil saturation under different imbibition systems is depicted in Fig. 5. The recovery curve of the four samples exhibits an initial slow increase, followed by rapid escalation. Combined with Table 2, after 48 h of imbibition, the recovery of AP, PP and MP of sample Y1 under the action of the ASW system are 1.89%, 1.95% and 3.28%, respectively. Meanwhile, for these three pore types, sample Y2 exhibits recoveries of -0.44%, 0.85% and 0, respectively, under the GBS system and sample Y3 shows -0.44%, 0.85% and 0 recoveries, respectively, under the CO_2 system. Sample Y4, treated with the S+ASW system, displays recoveries of 2.51%, 0.21% and -1.88%, respectively (Fig. 5(a)). These results suggest higher oil production in different pores under the ASW system at this stage. Following 192 hours of imbibition, the total recovery of the four samples rises by 9.01%-19.42%, with PP exhibiting the

highest increase ranging from 1.86% to 13.27%, AP showing an increase of 0.78%-9.53% across the four samples, while MP demonstrating the smallest increase, ranging from 0.01%-5.27%.

In general, upon the completion of imbibition, sample Y1 exhibits efficient crude oil production in AP, PP and MP, with recoveries of 5.82%, 6.78% and 3.54%, respectively. Sample Y2 predominantly produces oil in AP and MP, with recoveries of 9.09% and 2.71%, respectively. Sample Y3 demonstrates better production in PP and MP, with recoveries reaching 15.20% and 4.49%, respectively. Regarding sample Y4, higher degrees of oil production are observed in AP and PP, with recoveries of 7.76% and 6.00%, respectively. Interestingly, as depicted in Fig. 8(a), the MP recovery of samples Y3 and Y4 is negative, where the MP recovery initially decreases below zero before rising above it (Fig. 5(b)). This is due to the oil migration effect within the MP, that is, crude oil transfers from AP to larger pores under capillary forces, leading to the redistribution of remaining oil.

Fig. 5(c) illustrates the distribution of residual oil saturation during imbibition in different imbibition systems. Corresponding to the recovery curve, the residual oil saturation experiences slow decline in the early stage, followed by rapid change in the later stage. Collectively, after 192 h of imbibition treatment, the residual oil saturation in AP for the four shale samples is recorded at 82.90%, 85.81%, 47.55% and 80.24%, respectively. In comparison, the residual oil saturation in PP stands at 0.88%, 2.39%, 29.04% and 4.97%, while in MP, it is 0.09%, 0, 2.41% and 0.12%, respectively. Consequently, the total residual oil saturation amounts to 83.87%, 88.20%, 79.00% and 85.32%, respectively. Upon comparing samples Y1, Y2 and Y4, it is observed that the residual oil saturation of sample Y3 is decreased by 4.12%-5.79%. Notably, there is a significant reduction of 32.69%-38.26% in the residual oil saturation of AP and the residual oil is predominantly distributed in AP and PP less than 2 μm below the matrix, which can therefore serve as targets for continued potential extraction during post-imbibition development.

Essentially, the above findings indicate that both the ASW and GBS systems effectively enhance the hydrophilicity of
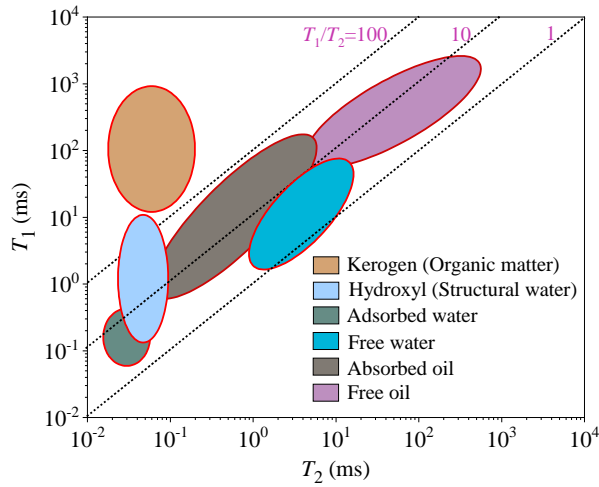
Fig. 6. 2D NMR T1-T2 occurrence state interpretation model.

Table 3. Division range of 2D NMR T_1-T_2 spectra of different hydrogen-containing components in shale reservoirs.

Hydrogen-containing components	Division range (ms)
Kerogen (Organic matter)	$T_2 < 1$, $T_1 > 10$, $T_1/T_2 > 100$
Hydroxyl (Structural water)	$T_2 < 0.2$, $T_1 < 10$, $T_1/T_2 = 1\text{-}100$
Adsorbed water	$T_2 < 0.2$, $T_1 > 0.05$, $T_1/T_2 = 1\text{-}10$
Free water	$T_2 < 10$, $T_1 > 0.1$, $T_1/T_2 = 1\text{-}10$
Absorbed oil	$T_2 \leq 33$, $T_1 \leq 100$, $T_1/T_2 = 15\text{-}150$
Free oil	$T_2 > 33$, $T_1 > 33$, $T_1/T_2 = 5\text{-}100$

the core, thereby reducing the oil-water interfacial tension in AP and MP and facilitating the efficient extraction of oil from different pore levels. When the CO_2 imbibition liquid enters the shale core, the CO_2 demonstrates notable regulatory effects on the oil-water interfacial tension. Under the action of diffusion, it can slowly imbibe into different levels of pores in the matrix, hence the pore oil can be recovered under imbibition extraction. Furthermore, in the case of sample Y4 under the action of S+ASW system, the AP oil recovery is 1.94% higher than that for sample Y1, attributable to the surfactant effectively reducing the oil-water interfacial tension of AP. However, this reduction in interfacial tension may also diminish the capillary pressure within relatively larger pores in the matrix, subsequently weakening the imbibition force and leading to a decrease in MP recovery and overall recovery. Therefore, when considering the application of surfactants in actual production, it becomes imperative to optimize their impact on reducing the oil-water interfacial tension while also ensuring the preservation of capillary pressure and imbibition power.

3.2 EOR of imbibition based on 2D NMR

3.2.1 Reconstruction of 2D NMR T_1-T_2 occurrence signal interpretation model

By exploiting the substantial variance in T_1 spectra among different hydrogen-containing components, we could delineate the 2D relaxation characteristic regions of these fluids within the shale cores by the addition of T_1 spectra to 1D T_2 spectra (Zhang et al., 2022). The methodology involves conducting a 2D NMR test on dried, water-saturated and oil-saturated core samples, analyzing the fluid composition changes, quantifying the signal variations of different hydrogen-containing components, and thereby determining the occurrence space of water and oil in saturated states, enabling the quantitative identification of fluids across various scales of reservoir space. By demarcating the ranges of different hydrogen-containing components on the T_1-T_2 2D spectrum, the occurrence state interpretation model of crude oil in shale reservoirs was constructed (Fig. 6). The findings reveal that shale oil occurs

primarily as kerogen (organic matter), hydroxyl (structural water), adsorbed water, free water, absorbed oil, and free oil, with the corresponding T_1-T_2 division ranges detailed in Table 3. Notably, the signal range for free oil is distributed where $T_2 > 33$ ms and $T_1 > 33$ ms, while adsorbed oil is characterized by $T_2 \leq 33$ ms and $T_1 \leq 100$ ms. The signals for organic matter are concentrated where $T_2 < 1$ ms and $T_1 > 10$ ms, with some overlap between adsorbed water and free water signals.

3.2.2 Imbibition occurrence state in different systems

Fig. 7 depicts the 2D NMR spectra of four samples in the dry state, saturated oil, and post-imbibition state. The expressions of relative recovery, absolute recovery and total recovery are shown in Eqs. (10)-(12). Consequently, the contribution of different crude oil occurrence states to EOR can be calculated according to the above 2D NMR signal interpretation model and Eqs. (10)-(12) (Table 4). It is found that the NMR signals of the four samples in the dry state are minimal, indicating that most residual oil can be extracted after core washing and drying, with a low remaining oil content within the core. Subsequently, upon oil saturation within the core, the signals for each occurrence state are substantially increased, with free and adsorbed oil constituting a significant proportion, while organic matter accounting for a smaller proportion. As imbibition progresses, the T_2 spectra of the four samples gradually shift to the left, accompanied by a gradual decline in the T_1 spectra. This trend signifies a progressive decrease in the signal of different occurrence states, with free oil production becoming more pronounced and residual oil transitioning dominantly to the adsorbed state and organic matter. Post-imbibition, a significant production of free oil is observed for the four samples, with relative recoveries of 32.73%, 27.36%, 25.40% and 31.25%, respectively. Considering the analysis results (Table 2 and Fig. 8), the PP, MP and microfractures in shale reservoirs can contribute to major oil recovery, thus the free oil in such pores can be effectively produced:

$$E_r = \frac{A_{ps} - A_{pd}}{A_s - A_d} \times 100\% \tag{10}$$

$$E_o = \frac{A_{ps} - PA_{pd}}{A_s} \times 100\% \tag{11}$$

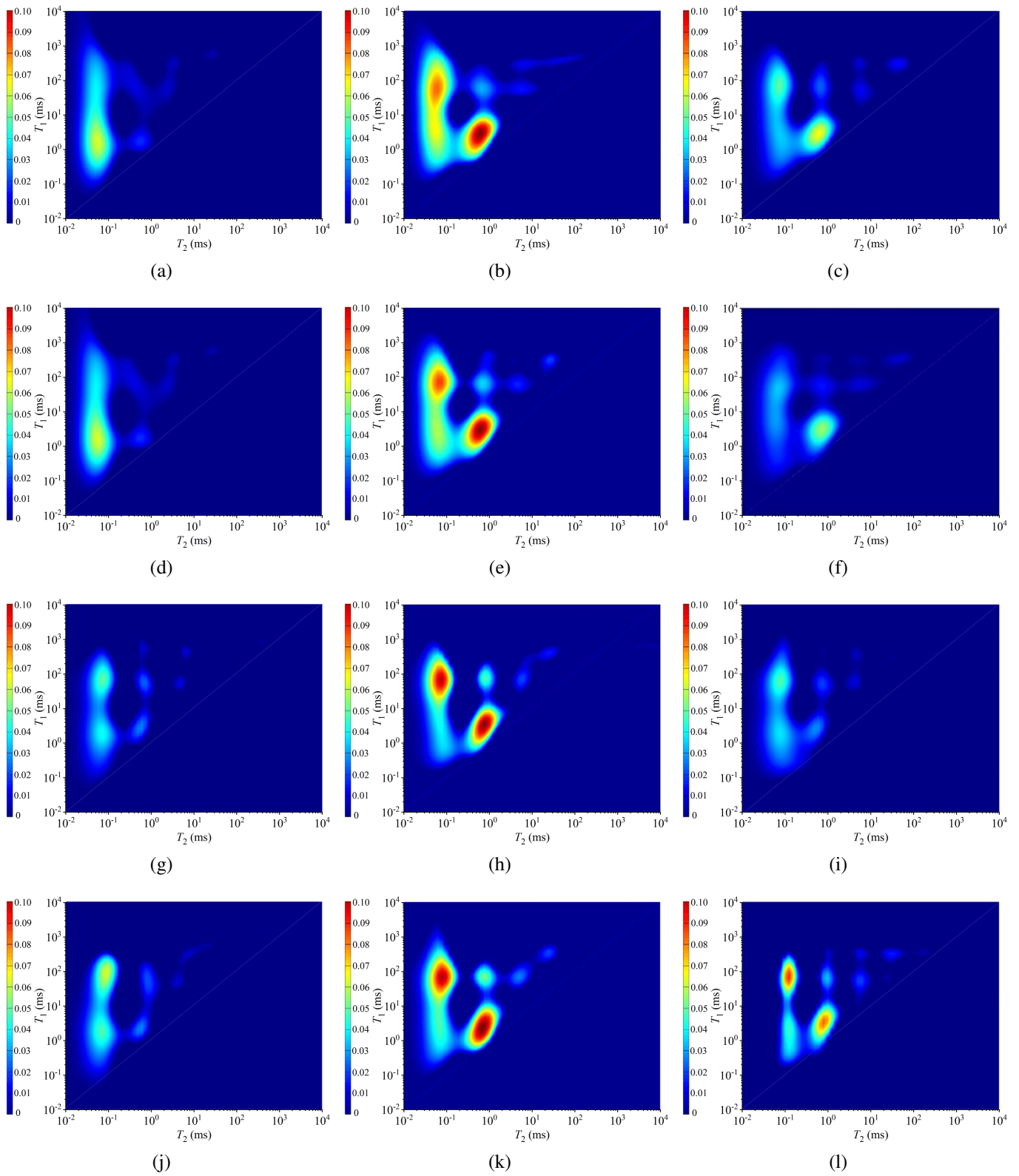$$E_t = \frac{A_s - A_d}{A_s} \times 100\% \tag{12}$$

Fig. 7. 2D NMR T_1-T_2 spectra of imbibition occurrence state evolution in different imbibition systems. (a)-(c) ASW system, (d)-(f) GBS system, (g)-(i) CO_2 system and (j)-(l) S+ASW system. From left to right, there are dry state, oil saturated and after imbibition, respectively.

Table 4. EOR imbibition experiment of different oil occurrence states.

Sample	Imbibition system	Occurrence state	Relative recovery (%)	Absolute recovery (%)	Total recovery (%)
Y1	ASW	Free oil	32.73	5.28	
		Absorbed oil	52.72	8.50	16.13
		Organic matter	14.55	2.35	
Y2	GBS	Free oil	27.36	3.27	
		Absorbed oil	55.69	6.52	11.80
		Organic matter	16.95	2.01	
Y3	CO_2	Free oil	25.40	5.33	
		Absorbed oil	36.51	7.66	21.00
		Organic matter	38.09	8.01	
Y4	S+ASW	Free oil	31.25	4.59	
		Absorbed oil	41.67	6.17	14.74
		Organic matter	27.08	3.98	

where E_r denotes the relative recovery, %; E_o denotes the absolute recovery, %; E_t denotes the total recovery, %; A_{ps} denotes the NMR signal of different oil occurrence states before imbibition, dimensionless; A_{pd} denotes the NMR signal of different oil occurrence states after imbibition, dimensionless; A_s denotes the total NMR signal of saturated oil before imbibition, dimensionless; A_d denotes the total NMR signal of saturated oil after imbibition, dimensionless.

Furthermore, under different imbibition systems, the relative recovery of adsorbed oil was 52.72%, 55.69%, 36.51% and 41.67%, respectively. Compared with the CO_2 system, water-based imbibition media (ASW, GBS) increased adsorbed oil recovery by 5.16%-19.18%. This can be attributed to the predominance of felsic siltstone and argillaceous siltstone lithologies in the study area. These lithologies are tight, with relatively high argillaceous clay content, leading to a large proportion of core adsorbed oil. Moreover, the small pore scale between clay layers enhances the imbibition capillary force, facilitating the effective production of adsorbed oil in shale reservoirs through wettability and capillary force mechanisms. The absolute recovery of adsorbed oil in the four samples was 8.50%, 6.52%, 7.66% and 6.17%, respectively, indicating the superior production effect of water-based imbibition media on adsorbed oil, consistent with their higher recovery rate for PP and AP oil. Importantly, the contribution of organic matter to oil recovery for the four samples reached 14.55%, 16.95%, 38.09% and 27.08%, respectively. In comparison with water-based systems, the CO_2 system increased organic matter oil recovery by 11.01%-23.54%. Besides, the correlation analysis aligned well with the changing trends observed in the 1D NMR T_2 spectrum. These results suggest that the CO_2 imbibition liquid can penetrate shale organic matter AP through diffusion and imbibition replacement to increase organic matter oil recovery. Consequently, the CO_2 system holds great promise as a favorable EOR technique in shale oil and storage consid-

erations.

3.3 Dynamic development of integrating injection-imbibition-soaking-production

Based on the NMR experimental results from various imbibition systems, it is evident that both the ASW and CO_2 systems yield higher oil recovery. In this section, we investigated the dynamic development characteristics and the contribution of different stages to recovery in the full-cycle development process of integrated injection-imbibition-soaking-production under matrix fracture coupling, and presented the results of online NMR dynamic seepage experiments conducted on samples Y5 (matrix-type) and Y6 (fracture-type) at various development stages.

3.3.1 Injection stage

Fig. 8 presents the 2D NMR T_1-T_2 spectra of Y5 samples at different development stages, and the different oil occurrence recovery is detailed in Table 5. Compared with the dry sample state, the 2D NMR spectrum signal of the core after saturated oil is significantly enhanced (Figs. 8(a) and 8(b)). Notably, the signal intensity is more pronounced in the fractured sample, indicating a higher occurrence of oil. Upon ASW liquid imbibition into the core, there is a slight decrease in the free oil signal in MP, while the adsorbed oil in AP exhibits an upward trend. Under different capillary pressure gradients, the imbibition liquid initially spreads to MP and microfractures due to its lower seepage resistance, resulting in a decrease in the free oil signal dominated by MP. Meanwhile, the imbibition liquid carries the oil in MP to AP and PP, causing a shift in the NMR T_1-T_2 spectral peak towards the smaller-scale pores on the left.
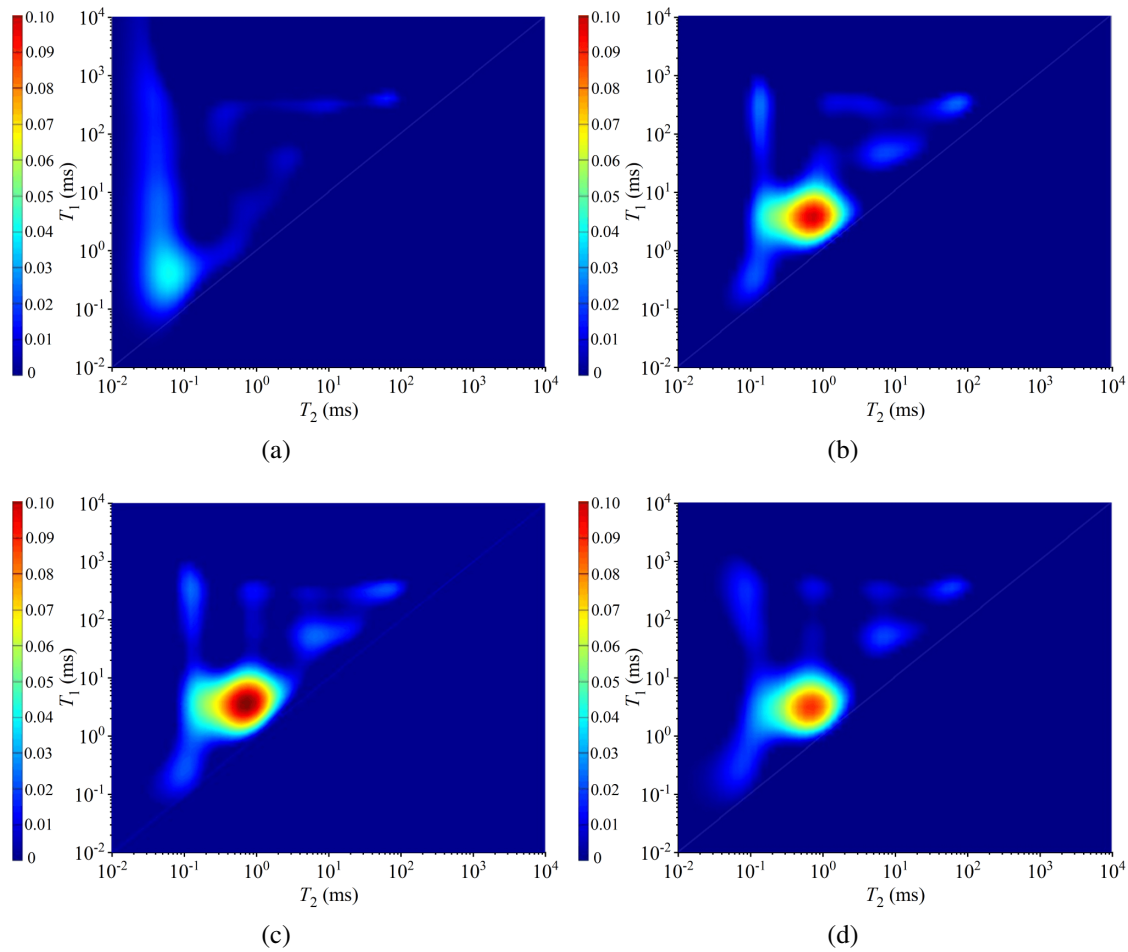
Fig. 8. 2D NMR spectra of matrix-type samples at different development stages. (a) Dry state, (b) oil saturated stage, (c) injection-imbibition stage and (d) soaking-production stage.

Table 5. Contribution of oil occurrence state to recovery for the ASW system, imbibition+CO_2 HNP.

Sample	State	Contribution of recovery				
		Imbibition	HNP	Imbibition+HNP relative recover (%)	Imbibition+HNP absolute recovery (%)	Total recovery (%)
Y5 (Matrix-type)	Free oil	15.04	6.20	76.19	21.24	
	Absorbed oil	3.10	1.77	17.46	4.87	27.88
	Organic matter	0.44	1.33	6.35	1.77	
L6 (Fractured-type)	Free oil	13.47	9.76	75.00	23.23	
	Absorbed oil	4.38	0.67	16.30	5.05	30.97
	Organic matter	1.68	1.01	8.70	2.69	

3.3.2 Imbibition stage

Fig. 9 shows the evolution of contributions from different oil occurrence states to recovery under different development stages. It is evident that the free oil dominated by MP and PP decreases significantly with time and the adsorbed oil dominated by clay interlayer pores and PP can also be gradually recovered under the action of imbibition stripping

(Fig. 8(c)). Following imbibition, the contributions of free oil, adsorbed oil and organic matter to recovery in the matrix core are 15.04%, 3.10% and 0.44%, respectively, while in the fractured core, these contributions were 13.47%, 4.38% and 1.68%, respectively (Fig. 9). The total recovery during the imbibition stage for the two sample types is 18.58% and 19.53%, respectively, indicating that the ASW system can ef-
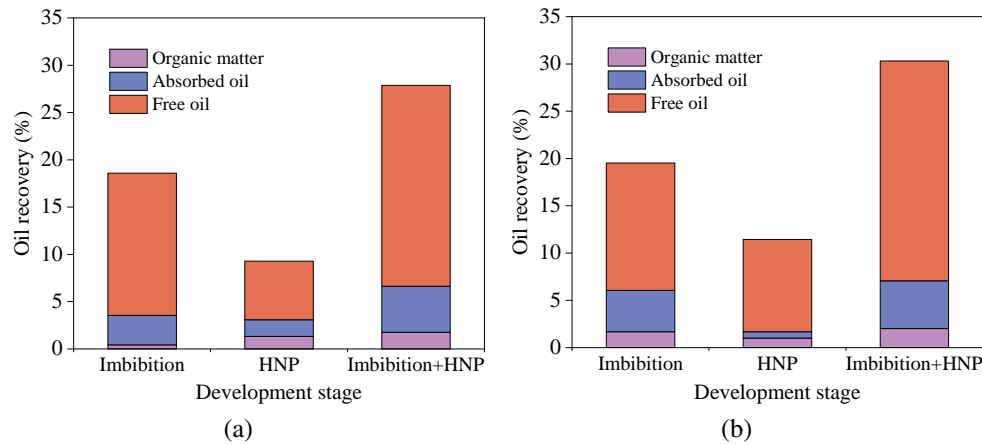
Fig. 9. Evolution of contribution of different oil occurrence states to recovery under different development stages. (a) Matrix-type sample and (b) fractured-type sample.

fectively EOR in the three types of oil. Overall, during the imbibition stage, free oil recovery is predominant and the contributions from absorbed oil and organic matter are relatively small. Notably, the matrix sample exhibits higher free oil recovery, while the fractured sample shows greater recoveries of adsorbed oil and organic matter. This disparity can be attributed to the fact that at the same wettability level, microfractures effectively increase the contact area between the matrix and imbibition liquid, thereby enhancing the production of adsorbed oil and organic matter through imbibition (Wang et al., 2020; Cai et al., 2021b; Huang et al., 2023). In practice, reservoir reconstruction technologies such as large-scale volume fracturing can effectively improve recovery by leveraging the dynamic imbibition oil production mechanism between matrix and fracture.

3.3.3 Soaking-production stage

Fig. 8(d) presents the 2D NMR T_1-T_2 spectra at different soaking-production stages. From the data, it is evident that with the repeated contact of CO_2 with oil in the soaking stage, the free oil dominating in MP and the organic matter dominating in AP shows a tendency to migrate to PP. This suggests that CO_2 can enter MP and AP under the pressure difference between matrix fractures, which makes the oil expansion caused by CO_2 diffusion increase the recovery of free oil and adsorbed oil. However, PP primarily facilitates oil migration, leading to a relatively lower recovery of adsorbed oil. During the huff production stage, as pressure decreases at the injection end, this notably increases the free oil yield. Through multiple cycles of CO_2 HNP, the adsorbed oil and organic matter are gradually produced by diffusion and carrying (Dai et al., 2019; Xu et al., 2023). In the puff stage, the interaction between oil and CO_2 takes place, such as diffusion and mass transfer, promoting the crude oil output in the puff stage by the action of dissolved gas flooding (Huang et al., 2023; Liu et al., 2023). After the end of HNP, the contributions of free oil, adsorbed oil and organic matter to recovery in the matrix core are 6.20%, 1.77% and 1.33%, respectively, while in the fractured core, these contributions are 9.76%, 0.67% and 1.01%, respectively.

The total recovery after the HNP stage for the two sample types is 27.88% and 30.97%, respectively, indicating that CO_2 HNP primarily enhances recovery through free oil, while there is relatively low recovery of adsorbed oil and an upward trend in organic matter recovery. It can be concluded that CO_2 can swiftly migrate along fractures into the matrix, achieving comparatively higher free oil recovery via miscible extraction.

3.3.4 Contribution of EOR in different development stages

In essence, although the injection stage of ASW imbibition medium contributes minimally to EOR, it facilitates the penetration of imbibition liquid into deeper core matrices, thereby enhancing energy storage and promoting the displacement of crude oil by imbibition. During the imbibition process, there is a notable increase in EOR for free and adsorbed oil, with marginal changes observed in organic matter recovery. In contrast to sample Y1, integrated full-cycle imbibition development for matrix and fracture samples yields a recovery increase of 2.45% and 3.40%, respectively, underscoring the pivotal role of imbibition displacement in enhancing shale recovery. Furthermore, compared with the imbibition stage, the CO_2 HNP stage significantly boosts EOR, as evidenced by a 9.30% and 11.44% increase in recovery for the matrix and fracture samples, respectively. This indicates that scattered residual oil within the core matrix can be effectively extracted through CO_2 stripping displacement and oil phase carrying mechanisms (Liu et al., 2024). From these results, it can be concluded that for fractured shale reservoirs, CO_2 soaking and HNP development after imbibition production are conducive to maximizing EOR. Overall, leveraging fluid imbibition displacement, energy storage and CO_2 displacement stripping and carrying effects emerges as a pivotal strategy for achieving optimal EOR.

4. Discussion

This study endeavors to bridge the gap between the microscopic pore crude oil production characteristics and the imbibition oil recovery mechanism in shale reservoirs and re-
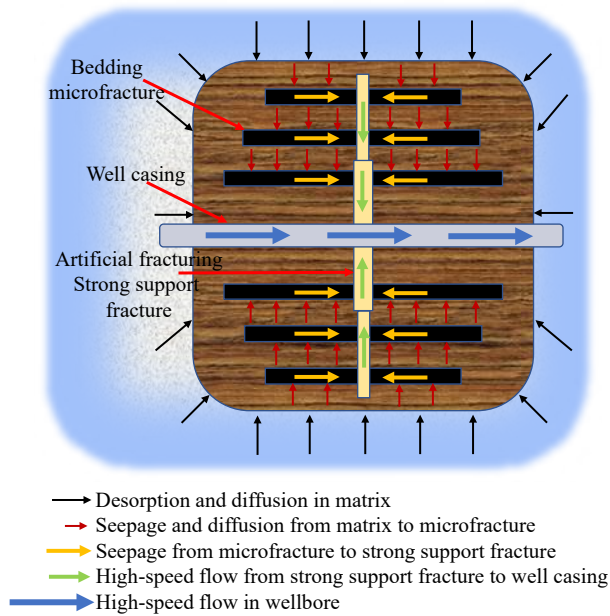
Fig. 10. Multiphase and multiscale oil migration seepage mechanism model under matrix fracture couplings.

lated research. Furthermore, it seeks to quantitatively study the dynamic development characteristics and mechanisms of different stages from the pore-scale perspective. To achieve these objectives, shale cores were subjected to imbibition NMR experiments in different imbibition systems. The production characteristics, residual oil distribution and EOR mechanism of crude oil in microscopic pores were quantitatively examined. Building on this foundation, an EOR scheme based on ASW imbibition coupled with CO_2 HNP was devised and the full-cycle integrated dynamic development characteristics of integrated injection-imbibition-soaking-production for different types of shale samples were elucidated. The findings have significant implications for theoretical analysis, numerical simulation and directional experimentation of the shale reservoir matrix-fracture coupling mode, opening up new avenues for further research.

Based on the aforementioned results from online NMR imbibition and HNP experiments, as well as the conceptual framework established for different modes of pore oil migration and production, the dynamic processes of imbibition and HNP within shale reservoirs involve the participation of microscopic pores of varying scales in the production process. This includes two distinct seepage modes: larger connected pores function as migration channels, while smaller pores contribute to seepage through oil-water imbibition. Accordingly, we established the multiphase and multiscale oil migration and the seepage mechanism model of shale oil reservoir with artificial fracturing strongly supporting the fracture-bedding fracture-matrix pore as the core (Fig. 10). Small pores in the matrix, characterized by strong seepage capacity and notable capillary pressure, allow the artificial fracture to connect with the bedding fracture when the shale reservoir undergoes fracturing (Tian et al., 2022; Li et al., 2023; Zou et al., 2024). During the imbibition and HNP process, crude oil is initially produced in the bedding fracture due to its high seepage capacity. As

production here declines, the small-pore oil in the matrix migrates towards micro-fractures, such as the bedding fracture through imbibition (Wang et al., 2020; Xu et al., 2023). Subsequently, the accumulated crude oil in the bedding fracture tends to migrate toward strongly supported artificial fractures. Therefore, micro-fractures can be considered as a bridge connecting the matrix pores with the strongly supported fractures, facilitating the flow of crude oil towards the wellbore and eventual production (Dai et al., 2019). Besides, the step-by-step flow pattern of matrix pore-bedding fracture-artificial fracture can significantly reduce the flow distance of fluid in a single medium and effectively reduce the seepage resistance.

5. Conclusions

In this study, a series of online NMR imbibition and HNP experiments were conducted while utilizing both 1D and T_1-T_2 2D online NMR techniques. The microscopic production characteristics and dynamic development characteristics were quantitatively studied at the pore scale. The main research conclusions are as follows:

1) Using the T_2 spectrum for shale reservoirs, based on occurrence, oil can be classed into adsorption pore oil, percolation pore oil and migration pore oil. The imbibition recovery of acidic low-viscosity slick water system, guar gum gel breaking solution system, CO_2 imbibition solution system and surfactant type acidic low-viscosity slick water system were 16.13%, 11.80%, 21.00% and 14.68%, respectively. Due to the dissolution reaction controlled by molecular diffusion, the CO_2 system demonstrated the most favorable development effect.

2) The different levels of pore oil exhibit varying microscopic production characteristics during imbibition. There is a positive correlation between the free oil recovery and the increased imbibition amount, the residual oil gradually shifts to adsorbed and organic matter-dominated forms and the recoverability decreases. Water-based imbibition media demonstrate a superior production effect for adsorbed oil in interlayered clay, whereas CO_2 imbibition media can effectively penetrate the AP of organic matter, facilitating mass transfer and imbibition replacement, leading to an enhanced recovery of 11.01%-23.54% for organic matter micropore oil.

3) Fractures prove instrumental in decreasing the migration resistance of pore oil and expanding the oil drainage area. For fractured shale reservoirs, CO_2 soaking and HNP development after imbibition production are conducive to maximizing EOR. Leveraging the bridge flow conductivity of fractures, fluid imbibition displacement and CO_2 carrying effect emerges as pivotal for achieving optimal EOR.

Acknowledgements

Conflict of interest

The authors declare no competing interest.

References

Afagwu, C., Alafnan, S., Mahmoud, M., et al. Modeling of natural gas self-diffusion in the micro-pores of organic-rich shales coupling sorption and geomechanical effects. Journal of Natural Gas Science & Engineering, 2022, 106: 104757.

Andersen, P. Insights from Boltzmann transformation in solving 1D counter-current spontaneous imbibition at early and late time. Advances in Geo-Energy Research, 2023, 7(3): 164-175.

Bocangel, W., Sondergeld, C., Rai, C. Acoustic mapping and characterization of organic matter in shales. Paper SPE 166331 Presented at the SPE Annual Technical Conference and Exhibition, New Orleans, Louisiana, USA, 30 September-2 October, 2013.

Cai, J. Some key issues and thoughts on spontaneous imbibition in porous media. Chinese Journal of Computational Physics, 2021a, 38(5): 505-512.

Cai, J., Jin, T., Kou, J., et al. Lucas-Washburn equation-based modeling of capillary-driven flow in porous systems. Langmuir, 2021b, 37: 1623-1636.

Dai, C., Cheng, R., Sun, X., et al. Oil migration in nanometer to micrometer sized pores of tight oil sandstone during dynamic surfactant imbibition with online NMR. Fuel, 2019, 245: 544-553.

Du, M., Lyu, W., Yang, Z., et al. An online physical simulation method for enhanced oil recovery by air injection in shale oil. Petroleum Exploration and Development, 2022, 49(5): 955-964.

Du, M., Yang, Z., Jiang, E., et al. Using digital cores and nuclear magnetic resonance to study pore-fracture structure and fluid mobility in tight volcanic rock reservoirs. Journal of Asian Earth Sciences, 2024, 259: 105890.

Fakher, S., Imqam A. Application of carbon dioxide injection in shale oil reservoirs for increasing oil recovery and carbon dioxide storage. Fuel, 2020, 265: 116944.

Fang, H., Li, A., Sang, S., et al. Numerical analysis of permeability rebound and recovery evolution with THM multi-physical field models during CBM extraction in crushed soft coal with low permeability and its indicative significance to CO_2 geological sequestration. Energy, 2023, 262: 125395.

Fu, C., Xu, X., Du, Y., et al. Experimental study on the influence of pore structure on spontaneous imbibition in marine black shale. Capillarity, 2024, 10(3): 57-72.

Gao, J., Kong, D., Peng, Y., et al. Pore-scale mechanisms and hysteresis effect during multi-cycle injection and production process in underground hydrogen storage reservoir. Energy, 2023, 283: 129007.

Ge, H., Yang, L., Shen, Y., et al. Experimental investigation of shale imbibition capacity and the factors influencing loss of hydraulic fracturing fluids. Petroleum Science, 2015, 12(4): 636-650.

Ghandi, E., Parsaei, R., Riazi, M. Enhancing the spontaneous imbibition rate of water in oil-wet dolomite rocks through boosting a wettability alteration process using carbonated smart brines. Petroleum Science, 2019, 16: 1361-1373.

Guo, G., Xue, X., Li, K., et al. Effect of retained fracturing fluid on the imbibition oil displacement efficiency of tight oil reservoir. Drilling Fluid & Completion Fluid, 2016, 33(6), 121-126. (in Chinese)

Guo, X., Semnani, A., Godwin A., et al. Experimental study of spontaneous imbibition for oil recovery in tight sandstone cores under high pressure high temperature with low field nuclear magnetic resonance. Journal of Petroleum Science and Engineering, 2021, 201: 108366.

Gu, X., Pu, C., Huang, H., et al. Micro-influencing mechanism of permeability on spontaneous imbibition recovery for tight sandstone reservoirs. Petroleum Exploration and Development, 2017, 44(6): 948-954.

Hosseini, M., Ali, M., Fahimpour, J. Energy storage in carbonate and basalt reservoirs: Investigating secondary imbibition in H_2 and CO_2 systems. Advances in Geo-Energy Research, 2024, 11(2): 132-140.

Huang, X., Tian, Z., Zuo, X., et al. The microscopic pore crude oil production characteristics and influencing factors by DME-assisted CO_2 injection in shale oil reservoirs. Fuel, 2023, 331: 125843.

Hu, Y., Zhao, C., Zhao, J., et al. Mechanisms of fracturing fluid spontaneous imbibition behavior in shale reservoir: A review. Journal of Natural Gas Science and Engineering, 2020, 82: 103498.

Jin, L., Hawthorne, S., Sorensen, J., et al. Advancing CO_2 enhanced oil recovery and storage in unconventional oil play-Experimental studies on Bakken shales. Applied Energy, 2017, 208: 171-183.

Jin, X., Du, M., Hao, C., et al. Characteristics and CO_2 flooding enhanced oil recovery experiments of Chang 6 in Ordos Basin. Petroleum Geology and Recovery Efficiency, 2024, 31(6): 1-13. (in Chinese)

Jin, Z., Zhu, R., Liang, X., et al. Several issues worthy of attention in current lacustrine shale oil exploration and development. Petroleum Exploration and Development, 2021, 48(6): 1276-1287.

Lai, F., Li, Z., Zhang, T., et al. Characteristics of microscopic pore structure and its influence on spontaneous imbibition of tight gas reservoir in the Ordos Basin, China. Journal of Petroleum Science and Engineering, 2019, 172: 23-31.

Li, C., Tan, M., Wang, Z., et al. Nuclear magnetic resonance pore radius transformation method and fluid mobility characterization of shale oil reservoirs. Geoenergy Science and Engineering, 2023, 221: 211403.

Li, S., Wang, Y., Deng, X., et al. Study on water displacement and imbibition features of Chang6 & Chang8 tight oil resevoir in Ordos Basin. Unconventional Oil & Gas, 2024, 11(2): 80-91. (in Chinese)

Li, W., Xu, S., Lu, C., Kinetics of spontaneous water-N_2 imbibition in carbon molecular sieves. Journal of Colloid

and Interface Science, 2019, 535: 28-32.

Liu, J., Sheng, J., Emadibaladehi, H., et al. Experimental study of the stimulating mechanism of shut-in after hydraulic fracturing in unconventional oil reservoirs. Fuel, 2021, 300: 120982.

Liu, Q., Li, J., Liang, B., et al. Complex wettability behavior triggering mechanism on imbibition: A model construction and comparative study based on analysis at multiple scales. Energy, 2023: 275: 127434.

Liu, Y., Fu, M., Wang, C., et al. Difference of damage to low permeability reservoirs by different injection methods of CO_2 flooding. Petroleum Geology and Recovery Efficiency, 2024, 31(2): 79-85. (in Chinese)

Lv, W., Chen, S., Gao, Y., et al. Evaluating seepage radius of tight oil reservoir using digital core modeling approach. Journal of Petroleum Science and Engineering, 2019, 178: 609-615.

Minh, C., Crary, S., Zielinski, L., et al. 2D-NMR applications in unconventional reservoirs. Paper SPE 161578 Presented at the SPE Canadian Unconventional Resources Conference, Calgary, Alberta, Canada, 30 October-1 November, 2012.

Nguyen, P., Willam, C., Viswanathan, H., et al. Effectiveness of supercritical-CO_2 and N2 huff-and-puff methods of enhanced oil recovery in shale fracture networks using microfluidic experiments. Applied Energy, 2018, 230(5): 160-174.

Qin, X., Cai, J., Wang, G., et al. Pore-scale modeling of pore structure properties and wettability effect on permeability of low-rank coal. International Journal of Mining Science and Technology, 2023, 5: 573-584.

Sharma, J., Inwood, S., Kovscek, A. Experiments and analysis of multiscale viscous fingering during forced imbibition. SPE Journal, 2012, 17(4): 1142-1159.

Singh, H., Cai, J. Screening improved recovery methods in tight-oil formations by injecting and producing through fractures. International Journal of Heat and Mass Transfer, 2018, 116: 977-993.

Tian, Z., Wei, W., Zhou, S., et al. Impacts of gas properties and transport mechanisms on the permeability of shale at pore and core scale. Energy, 2022; 244:122707.

Wang, C., Gao, H., Qi, Y., et al. Investigation on the mechanisms of spontaneous imbibition at high pressures for tight oil recovery. ACS Omega, 2020, 5(22): 12727-12734.

Wang, J., Liu, H., Xia, J., et al. Mechanism simulation of oil displacement by imbibition in fractured reservoirs. Petroleum Exploration and Development, 2017, 44(5): 761-770.

Wang, J., Salama, A., Kou, J., Experimental and numerical analysis of imbibition processes in a corrugated capillary tube. Capillarity, 2022, 5(5): 83-90.

Wang, Y., Shang, Q., Guo, J., et al. Study on imbibition during the CO_2 enhanced oil recovery in fractured tight sandstone reservoirs. Capillarity, 2023, 7(3): 47-56.

Washburn, E. W. The dynamics of capillary flow. Physical Review, 1921, 17(3): 273-283.

Wei, J., Zhang, D., Zhang, X., et al. Experimental study on water flooding mechanism in low permeability oil reservoirs based on nuclear magnetic resonance technology. Energy, 2023a, 278: 127960.

Wei, X., Fu, L., Zhao, G., et al. Nuclear magnetic resonance study on imbibition and stress sensitivity of lamellar shale oil reservoir. Energy, 2023b, 282: 128872.

Xiong, X., Sheng, J., Wu, X., et al. Experimental investigation of foam-assisted N_2 huff-n-puff enhanced oil recovery in fractured shale cores. Fuel, 2022, 311: 122597.

Xu, L., Li, Q., Myers, M., et al. Investigation of the enhanced oil recovery mechanism of CO_2 synergistically with nanofluid in tight glutenite. Energy, 2023, 273: 127275.

Yang, M., Huang, S., Zhao, F., et al. Experimental investigation of CO_2 huff-n-puff in tight oil reservoirs: Effects of the fracture on the dynamic transport characteristics based on the nuclear magnetic resonance and fractal theory. Energy, 2024, 294: 130781.

Yang, Z., Liu, X., Li, H., et al. Analysis on the influencing factors of imbibition and the effect evaluation of imbibition in tight reservoirs. Petroleum Exploration and Development, 2019, 46(4): 739-745.

Zhang, T., Tang, M., Ma, Y., et al. Experimental study on CO_2/water flooding mechanism and oil recovery in ultralow-permeability sandstone with online LF-NMR. Energy, 2022, 252: 123948.

Zhao, M., He, H., Dai, C., et al. An EOR study of a new mobility control system on the dynamic imbibition in a tight oil fracture network model. Energy Fuels, 2018, 32(3): 2908-2915.

Zhou, Y., Guan, W., Zhao, C., et al. Spontaneous imbibition behavior in porous media with various hydraulic fracture propagations: A pore-scale perspective. Advances in Geo-Energy Research, 2023, 9(3): 185-197.

Zhou, Y., Guan, W., Zhao, C., et al. Numerical methods to simulate spontaneous imbibition in microscopic pore structures: A review. Capillarity, 2024, 11(1): 1-21.

Zou, S., Chen, D., Kang, N. An experimental investigation on the energy signature associated with multiphase flow in porous media displacement regimes. Water Resources Research, 2024, 60: e2023WR036241.